Closed form solution for *Fatemi-Socie* critical plane method in case of linear elasticity and proportional loading

Andrea Chiocca[a,*], Michele Sgamma[a], Francesco Frendo[a]

[a]*Department of Civil and Industrial Engineering, University of Pisa, Pisa, Italy*

Abstract

The fatigue analysis of structural components is a relevant research topic in both scientific and industrial communities. Despite major advances in understanding, fatigue damage remains a significant issue for both metallic and non-metallic components, sometimes leading to unexpected failures of in-service parts. Among the different assessment methodologies, critical plane methods have gained significance as they enable identification of a component's critical location and direction of early crack propagation. However, the standard plane scanning method for calculating critical plane factors is computationally intensive and, for that, it is only applied when the component critical regions are already known. When critical areas are not easily identifiable due to complex geometries, loads or constraints, a more efficient method for evaluating critical plane factors would be required. This work presents a closed form solution for efficiently evaluating the Fatemi-Socie critical plane factor, in case of linear-elastic material behaviour and proportional loading conditions, based on tensor invariants and coordinates transformation laws. The proposed algorithm was tested on different test cases (i.e. hourglass, notched and welded joint geometries) under different loading conditions (i.e. tensile, bending and torsion) and showed a significant reduction in computation time compared to the standard plane scanning method.

Keywords: critical plane approach, Fatemi-Socie, fatigue analysis, computational cost, efficient algorithm, speed-up calculation, closed form solution

Nomenclature

$\alpha^1, \alpha^2, \alpha^3$	Eigenvalues
$\boldsymbol{\Delta\varepsilon}^{(i,i+1)}$	Strain range tensor between the i-th and $i+1$-th load steps
$\boldsymbol{\sigma'}$	Rotated stress tensor
$\boldsymbol{\sigma}$	Stress tensor
$\boldsymbol{\sigma}^{(i)}$	Stress tensor at the i-th load step
$\boldsymbol{\varepsilon'}$	Rotated strain tensor
$\boldsymbol{\varepsilon}$	Strain tensor
$\boldsymbol{\varepsilon}^{(i)}$	Strain tensor at the i-th load step
$\boldsymbol{n_j}^{(i),(i+1)}$	j-th principal direction of the strain range tensor
$\Delta\gamma$	Range of shear strain
$\Delta\theta$, $\Delta\psi$	Fixed angular increment
γ_{ij}	Shear strain
ν	Poisson's ratio
ω	Angle of the principal reference frame rotation
σ_{ij}	Normal stress

*Corresponding author

Email addresses: andrea.chiocca@unipi.it (Andrea Chiocca), michele.sgamma@phd.unipi.it (Michele Sgamma), francesco.frendo@unipi.it (Francesco Frendo)

$\sigma_{n,max}$	Maximum normal stress
τ_{ij}	Shear stress
θ, ψ	Standard scanning plane angles
ε_{ij}	Normal strain
$a\,b\,c\,d$	Analytical formula parameters
E	Young's modulus
F	Force
k	*Fatemi-Socie* material constant
M_t	Torque
$Oxyz$	Reference coordinate system
R	Rotation matrix
R_i	Rotation matrix around i-axis
S_y	Yield strength
t_{cs}	Computation time for the closed form solution
t_{ps}	Computation time for the plane scanning procedure
FS	*Fatemi-Socie* critical plane factor
PI	Performance index
CP	Critical Plane
FEA	Finite Element Analysis
FEM	Finite Element Model

1. Introduction

The investigation of material's fatigue damage is a strategic subject of major relevance in several areas including academia and industry. Cumulative in-service fatigue loading is still one of the major causes of unexpected failures [1], and it represents an important issue for designers. Although fatigue tests are often represented by simplified analyses, complexities such as stress/strain gradients, variable amplitude loading, randomness and multiaxiality can easily be encountered in real cases [2]. Especially in such circumstances, finite element analysis (FEA) provides a valuable tool able to account for the complex features mentioned above [3–8]. The standard way to approach fatigue analysis consists of investigating the component's critical regions (i.e. considering stress/strain gradients and multiaxiality), and applying the correct loading history (i.e. accounting for variable amplitude or randomness). However, given the wide variety of geometries, loading conditions, and damage parameters to be considered, the solution of such models can be time-consuming during both the solution and post-processing phases.
While the complexity of geometry and boundary conditions is inherently related to the investigated problem and therefore unavoidable, the selection of the damage parameter, on the other hand, is a designer choice. Several methods exist to assess fatigue damage, among them two macro-categories can be identified: energy-based methods [9–12] and stress or strain-based methods [13–21]. Among the above mentioned categories, in the context of local damage methods, critical plan (CP) approaches gained a lot of popularity in recent years [22–26]. Methods based on critical plane require evaluating the plane orientation which is subjected to the most severe damage. This orientation is defined as the critical plane and is representative of the orientation, at the material specific location, over which the crack should nucleate and initially propagate. Especially for the implementation of such damage parameters, the use of FEM is of great use when dealing with complex geometry and complicated loading histories. The standard way of evaluating the critical plane factor, however, requires the calculation of the damage factor over all possible plane orientations at each node of a FE model identifying the critical plane through a blind-search for scanning process. Each plane orientation is identified by a set of two or three angles which are varied discretely by a fixed angular step to cover all the three-dimensional space. The processes is carried on for each node of the FE-model, usually throughout nested *for/end* loops, thus, requiring significant computational power. Yet, the wide potential arising from such methodologies is currently limited due to their cumbersome implementation and, if compared to other widespread damage factors (e.g., nominal stress, hot spot stress, notch stress approach, etc.), critical plane methods are still confined to research and academia, being rarely used in the industry. The extensive computation time causes that only the critical zone of a component (e.g., notch) can be directly examined. However, this area may not always be identifiable *a priori* due to possible complex

geometries, load histories and constraints.
The main challenge during the computational process is to set the angular increment finding the right balance between accuracy and efficiency. Previous researches have focused on reducing the time needed for critical plane factor calculations. Some methods use analytical or semi-analytical techniques to determine the damage factor and the direction where it is maximized. A novel algorithm presented by Marques et al. [27] utilizes analytical formulas to calculate only the spectral parameters related to the damage factor. Other approaches aim to increase computational speed by only calculating the critical plane factor in specific planes, rather than discretizing the entire space. Wentingmann et al. [28] have developed an algorithm that increases the speed of critical plane detection by segmenting a coarse Weber half sphere with quad elements. Similarly, Sunde et al. [29] developed an adaptive scheme that densifies a triangular mesh around the elements where the greatest damage has been observed. Sometimes instead, the loading condition of the specimen results in a reduced stress state that allows for a purely analytical formulation of the damage factor [30–32].
This paper represents an extension of a previous paper by the authors (Chiocca et al. [33]), where an analytical formulation to efficiently apply the critical plane method was developed for parameters that require the maximization of a single factor is required (e.g. the original formulation of *Fatemi-Socie*, which is based on the maximun shear strain range, *Smith-Watson-Topper*, *Kandil–Brown–Miller* , etc.). The analytical model presented in the following refers to the more general *Fatemi-Socie* formulation according to Jiang et al. [34], which is based on a combination of shear strain range and normal stress. Also in this case, indeed, under the assumption of proportional loading and linear-elastic material, a closed form solution is possible. The model has been developed to be applied together with finite element analyses; for this reason the constituent mathematics is based on a discrete formulation of the time history and the stress and strain tensors are defined for each generic loading condition. In the case of a complex load history, the method can be iteratively applied to each successive peak-to-valley, valley-to-peak pair derived from a specific cycle counting formulation. The first part of the paper explains the methodology in details, providing the necessary theoretical background. In the second part of the paper, case studies are presented, including an hourglass specimens, notched specimens and welded components under different loading conditions. A comparison is made between the standard method of calculating CP factors (i.e. plane scanning method) and the methodology presented in this work, in terms of solution accuracy and computational cost.

2. General background on CP factors evaluation

The present paper aims at obtaining an analytcal solution for the general formulation of the *Fatemi-Socie* CP factor (FS) [18] as proposed in [34] and given by:

$$FS = \frac{\Delta\gamma}{2}\left(1 + k\frac{\sigma_{n,max}}{S_y}\right) \tag{1}$$

In previous equation $\Delta\gamma$ represents the range of shear strain, $\sigma_{n,max}$ the maximum (i.e. over the load cycle/time interval) normal stress on the plane being evaluated, and S_y the material's yield strength. The material parameter k can be determined by comparing fatigue experimental data for uniaxial loading with data for pure torsion as described in [35]. Although certain authors suggest that the additional parameter k varies with the number of cycles to failure [36–39], a constant value was considered for the present study. The FS parameter is a positive parameter, based on the fact that the shear strain range is considered in absolute value and considering that only positive normal stresses are taken into account.
The simpler formulation of the FS parameter, which focuses on maximizing the range of shear strain only (as originally proposed in [18, 40]) has been the subject of a previous paper by the authors [33]. In this work a method is developed, which aims at finding a closed form solution for the maximum of the whole FS parameter, i.e. the critical plane is defined as that particular plane, among all possible orientations at a given location, for which the expresion given in eq. 1 reaches its maximum value.

3. Evaluating the CP factor using standard plane scanning technique

In this section, the standard procedure for determining the CP factor through the plane scanning technique is briefly recalled. The time-varying stress $\boldsymbol{\sigma}(t)$ and strain $\boldsymbol{\varepsilon}(t)$ tensors can be calculated at every node in a FE model in a general, generally global, reference system $Oxyz$.

$$\boldsymbol{\sigma}(t) = \begin{bmatrix} \sigma_{xx}(t) & \tau_{xy}(t) & \tau_{xz}(t) \\ \tau_{yx}(t) & \sigma_{yy}(t) & \tau_{yz}(t) \\ \tau_{zx}(t) & \tau_{zy}(t) & \sigma_{zz}(t) \end{bmatrix}, \; \boldsymbol{\varepsilon}(t) = \begin{bmatrix} \varepsilon_{xx}(t) & \frac{\gamma_{xy}}{2}(t) & \frac{\gamma_{xz}}{2}(t) \\ \frac{\gamma_{yx}}{2}(t) & \varepsilon_{yy}(t) & \frac{\gamma_{yz}}{2}(t) \\ \frac{\gamma_{zx}}{2}(t) & \frac{\gamma_{zy}}{2}(t) & \varepsilon_{zz}(t) \end{bmatrix} \tag{2}$$

Stress and strain tensors can be utilized to describe various types of loading conditions, such as multiaxial, uniaxial, or biaxial conditions, and can also exhibit proportional or non-proportional stress components depending on the load history. It is possible to calculate stress and strain values acting on different plane orientations, i.e. with reference to different reference coordinate systems, by simple matrix operation $R^T \boldsymbol{\sigma} R$, where R represents the rotation matrix, which is usually expressed by three different angles (e.g., *Euler, Briant, Cardano*). Actually, two angular coordinates, say θ and ψ, are strictly necessary to identify a plane orientation, the third rotation simply representing a rotation about the unit vector $\mathbf{n}$, which is orthogonal to the plane. In this sense there are ∞^2 possible orientation at each location to be checked. By incrementally rotating the plane (or its unit vector) through fixed angular increments (i.e., $\Delta\theta$ and $\Delta\psi$), stress and strain values in all directions can be approximately obtained. Once this process has been carried out, the plane that maximizes the reference CP parameter can be identified as the critical plane. The above mentioned procedure requires to implement nested *for/end* loops and this results highly inefficient from a computational point of view, depending on the selected angular resolution. This becomes even more critical when trying to perform this analysis for many points in the component (i.e., nodes in the FE model).

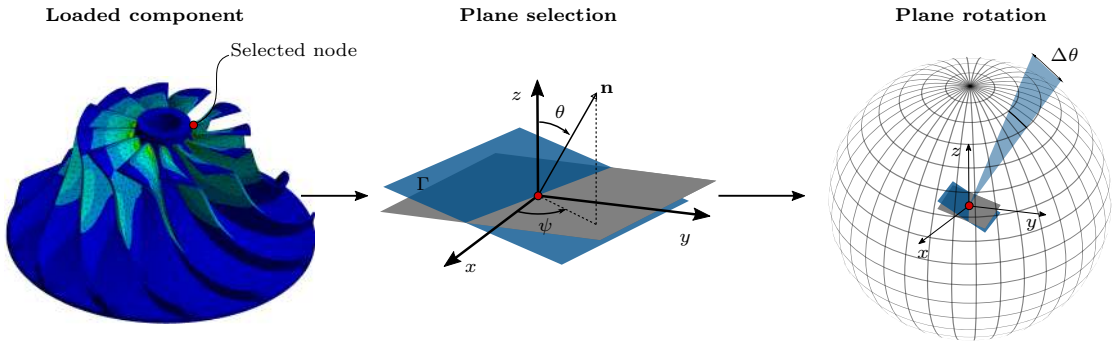

Figure 1: Standard procedure sequence to assess a critical plane factor by plane scanning method

For the present study a rotation sequence in a moving frame of reference was taken as a reference, the first rotation θ around the z-axis and the second rotation ψ around the y-axis, as shown in Equation 3 and the plane scanning method was applied through angular steps $\Delta\theta$ and $\Delta\psi$ of 1°.

$$R = R_z(\psi)R_y(\theta) = \begin{bmatrix} \cos(\theta)\cos(\psi) & -\sin(\psi) & \cos(\psi)\sin(\theta) \\ \sin(\psi)\cos(\theta) & \cos(\psi) & \sin(\theta)\sin(\psi) \\ -\sin(\theta) & 0 & \cos(\theta) \end{bmatrix} \tag{3}$$

Through the rotation matrix R it is possible to retrieve the stress and strain tensors in the rotated reference frame as presented in Equation 15.

$$\boldsymbol{\sigma'} = R^T \boldsymbol{\sigma} R, \; \boldsymbol{\varepsilon'} = R^T \boldsymbol{\varepsilon} R \tag{4}$$

4. Closed form solution for whole *Fatemi-Socie* CP factor

In this section the mathematical framework of the method is outlined. As the method was developed for a finite element modeling-related application, the load history is described by a discrete formulation of

the time sequence, via load steps in a FE-analysis. To this regard, relationships 5 give the stress and strain tensors at the generic i-th loading step.

$$\boldsymbol{\sigma}^{(i)} = \begin{bmatrix} \sigma_{xx} & \tau_{xy} & \tau_{xz} \\ \tau_{yx} & \sigma_{yy} & \tau_{yz} \\ \tau_{zx} & \tau_{zy} & \sigma_{zz} \end{bmatrix}^{(i)} , \; \boldsymbol{\varepsilon}^{(i)} = \begin{bmatrix} \varepsilon_{xx} & \frac{\gamma_{xy}}{2} & \frac{\gamma_{xz}}{2} \\ \frac{\gamma_{yx}}{2} & \varepsilon_{yy} & \frac{\gamma_{yz}}{2} \\ \frac{\gamma_{zx}}{2} & \frac{\gamma_{zy}}{2} & \varepsilon_{zz} \end{bmatrix}^{(i)} \tag{5}$$

Starting from the above tensors, the strain range tensor between the i-th and $i+1$-th loading conditions can be easily determined, as shown in Equation 6; in order to compute the strain range tensor, the starting tensors have to be defined with respect to the same reference system, but this is fairly common within the post-processing phase of FE-analyses.

$$\boldsymbol{\Delta\varepsilon}^{(i,i+1)} = \boldsymbol{\varepsilon}^{(i)} - \boldsymbol{\varepsilon}^{(i+1)} = \begin{bmatrix} \Delta\varepsilon_{xx} & \frac{\Delta\gamma_{xy}}{2} & \frac{\Delta\gamma_{xz}}{2} \\ \frac{\Delta\gamma_{yx}}{2} & \Delta\varepsilon_{yy} & \frac{\Delta\gamma_{yz}}{2} \\ \frac{\Delta\gamma_{zx}}{2} & \frac{\Delta\gamma_{zy}}{2} & \Delta\varepsilon_{zz} \end{bmatrix}^{(i,i+1)} \tag{6}$$

Under the hypotheses of linear elasticity and proportional loading the following considerations hold:

- the stress and strain tensors have the same principal directions, i.e. the same eigenvectors;
- the strain tensors (as well as the stress tensor), evaluated at different time steps, (i) and $(i+1)$ have the same principal directions, i.e. the same eigenvectors.

From the above considerations it follows that also the strain range tensor (as well as, for example the stress range tensor for the *Findley* criterium) $\boldsymbol{\Delta\varepsilon}^{(i,i+1)}$ has the same principal directions of the strain or the stress tensors, evaluated at the i-th and $i+1$-th time step.

On the basis of the coincidence between the principal directions of the tensors $\boldsymbol{\sigma}^{(i)}$, $\boldsymbol{\sigma}^{(i+1)}$, $\boldsymbol{\varepsilon}^{(i)}$, $\boldsymbol{\varepsilon}^{(i+1)}$ and $\boldsymbol{\Delta\varepsilon}^{(i,i+1)}$, it is now useful to refer to the Mohr's circular representation to further illustrate the method. Figure 2 represents the tensor quantities which are present in the *Fatemi-Socie* critical plane method (see eq. 1), namely $\boldsymbol{\Delta\varepsilon}^{(i,i+1)}$, $\boldsymbol{\sigma}^{(i)}$ and $\boldsymbol{\sigma}^{(i+1)}$. As a first step all the stress and strain components have to be obtained (at a given node in the FE model) in a given, typically the global, reference frame $Oxyz$. Then, an *eigenvalue–eigenvector* analysis is required for the strain range tensor $\boldsymbol{\Delta\varepsilon}^{(i,i+1)}$; the so obtained *eigenvalues* represent the principal parameters of the strain range $\Delta\varepsilon_1^{(i,i+1)}$, $\Delta\varepsilon_2^{(i,i+1)}$ and $\Delta\varepsilon_3^{(i,i+1)}$, while the *eigenvectors* will define the principal directions $\mathbf{n_1}^{(i),(i+1)}$, $\mathbf{n_2}^{(i),(i+1)}$ and $\mathbf{n_3}^{(i),(i+1)}$ of the $\boldsymbol{\Delta\varepsilon}^{(i,i+1)}$ tensor. As previously stated, these unit vectors also represent the principal directions (i.e. *eigenvectors*) of the tensors $\boldsymbol{\sigma}^{(i)}$ and $\boldsymbol{\sigma}^{(i+1)}$. Therefore, the three tensors $\boldsymbol{\Delta\varepsilon}^{(i,i+1)}$, $\boldsymbol{\sigma}^{(i)}$ and $\boldsymbol{\sigma}^{(i+1)}$ expressed in the principal reference frame $On_1n_2n_3$ are represented by their principal components (i.e. *eigenvalues*) ($\Delta\varepsilon_1^{(i,i+1)}$, $\Delta\varepsilon_2^{(i,i+1)}$, $\Delta\varepsilon_3^{(i,i+1)}$), ($\sigma_1^{(i)}$, $\sigma_2^{(i)}$, $\sigma_3^{(i)}$) and ($\sigma_1^{(i+1)}$, $\sigma_2^{(i+1)}$, $\sigma_3^{(i+1)}$), with the usual convention $\alpha^1 > \alpha^2 > \alpha^3$, α representing the generic *eigenvalue*.
Finally, on the basis of the Mohr's circular representation, the FS parameter can be obtained as follows. The analytical expression of $\frac{\Delta\gamma}{2}^{(i,i+1)}$, as a function of the ω angle, which represents a rotation around the n_2 principal direction (see Figure 2), is given by the following relationship 7.

$$\frac{\Delta\gamma^{(i,i+1)}(\omega)}{2} = \left(\frac{\Delta\varepsilon_1^{(i,i+1)} - \Delta\varepsilon_3^{(i,i+1)}}{2} \right) \sin(2\omega) \tag{7}$$

Considering the normal stress acting on the plane identified by the ω angle, the maximum value among the two conditions (i) and $(i+1)$ of the load cycle have to be considered:

$$\sigma_{n,max}^{(i),(i+1)}(\omega) = \max_{\{(i),(i+1)\}} \left[\left(\frac{\sigma_1 + \sigma_3}{2} \right) + \left(\frac{\sigma_1 - \sigma_3}{2} \right) \cos(2\omega) \right]^{(i),(i+1)} \tag{8}$$

From Fig. 2 it can be observed that the maximum normal stress can belong either to the (i)-th time step, or the $(i+1)$-th time step, depending on the plane orientation ω.

In order to solve the following maximization problem, represented by Equation 9,

$$FS(\omega) = \max_{\{\omega\}} \left[\frac{\Delta\gamma^{(i,i+1)}(\omega)}{2} \left(1 + k \frac{\sigma_{n,max}^{(i),(i+1)}(\omega)}{S_y} \right) \right] \tag{9}$$

the following parameters are introduced:

$$\begin{cases} a = \left(\frac{\Delta\varepsilon_1^{(i,i+1)} - \Delta\varepsilon_3^{(i,i+1)}}{2} \right) \\ b = \left(\frac{\sigma_1 + \sigma_3}{2S_y} \right)^{(i),(i+1)} \\ c = \left(\frac{\sigma_1 - \sigma_3}{2S_y} \right)^{(i),(i+1)} \\ d = \left(\sqrt{k^2 \left(b^2 + 8c^2 \right) + 2bk + 1} \right)^{(i),(i+1)} \end{cases} \tag{10}$$

Parameter a represents the diameter of the largest strain range circle in Figure 2; parameter b represent the center of the largest stress circle, normalized with respect to the yield stress; parameter c represents the diameter of the largest stress circle, normalized with respect to the yield stress; d is a combination of previous parameters and the material constant k. It should be noted that a is referenced to the load cycle, while b, c and d has to be evaluated for (i)-th and $(i+1)$-th time step. Parameters a and c are always positive according to the standard convention on the *eigenvalues* ($\Delta\varepsilon_1 \geq \Delta\varepsilon_2 \geq \Delta\varepsilon_3$ and $\sigma_1 \geq \sigma_2 \geq \sigma_3$), while b can be either positive or negative.

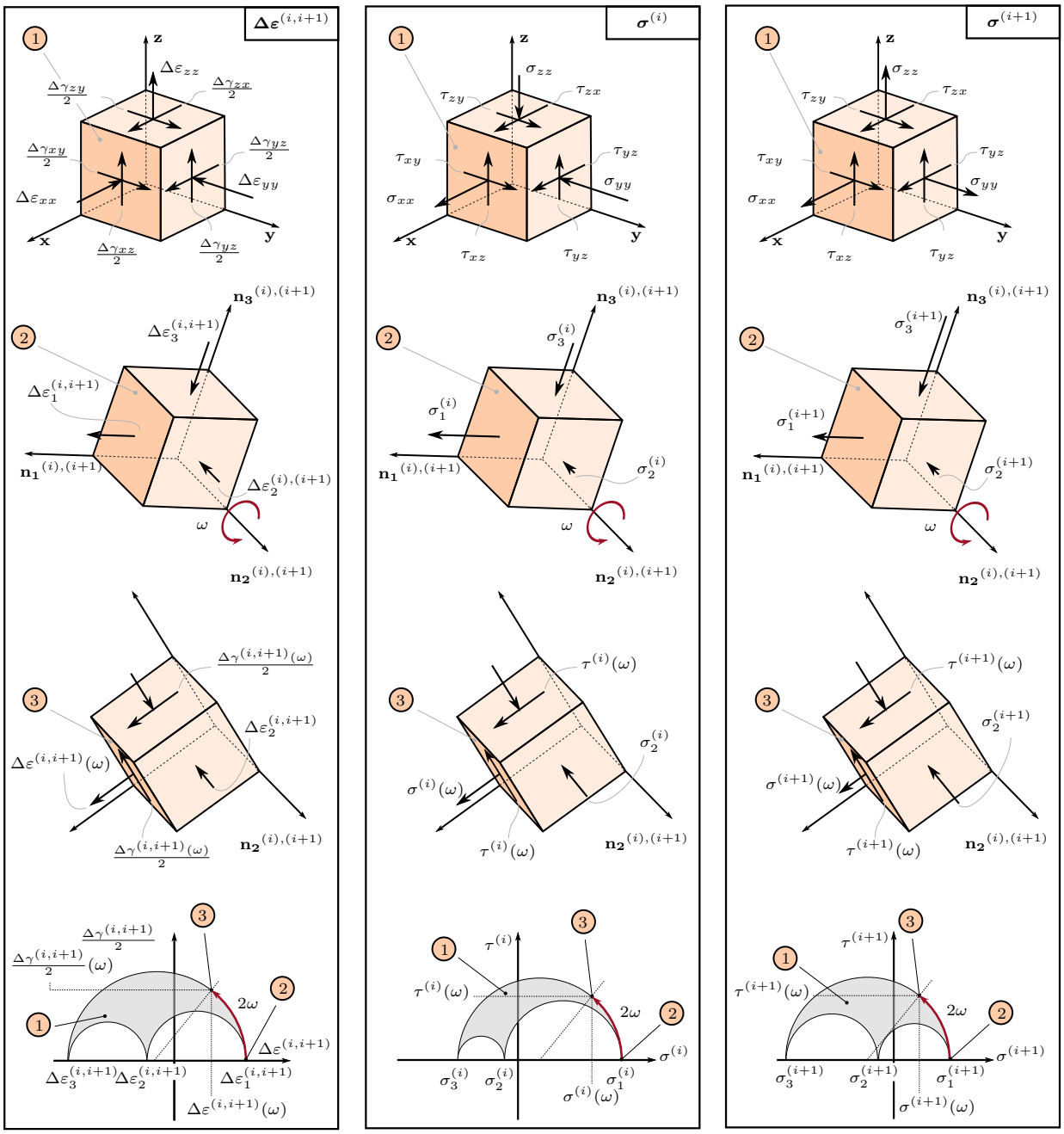

Figure 2: Graphical representation of the analytical method by Cauchy elementary cube and Mohr's circle by means of the tensors $\boldsymbol{\Delta\varepsilon}^{(i,i+1)}$, $\boldsymbol{\sigma}^{(i)}$ and $\boldsymbol{\sigma}^{(i+1)}$

After substituting expressions 10 into relationship 9, the maximum value of FS parameter can be determined by carrying out an analytical derivative of the $FS(\omega)$ function with respect to ω, as presented in the Equation 11.

$$FS(\omega) = \max_{\{\omega\}} \left[a \sin(2\omega) \left(1 + k(b + c\cos(2\omega))\right)\right] \tag{11}$$

The result of that analysis in terms of ω_{max} and FS_{max} are given in the following Equations 12–13:

$$\omega_{max} = \begin{cases} \frac{1}{2}\arctan\left(\dfrac{\frac{\sqrt{2}\sqrt{\frac{k\left(b(d-2)+b^2(-k)+4c^2k\right)+d-1}{ck}}}{\sqrt{c}\sqrt{k}}}{\frac{d-bk-1}{ck}}\right) & b \geq -\frac{1}{k} \\ \frac{1}{2}\arctan\left(\dfrac{-\frac{\sqrt{2}\sqrt{-\frac{k\left(b(d+2)+b^2k-4c^2k\right)+d+1}{ck}}}{\sqrt{c}\sqrt{k}}}{-\frac{d+bk+1}{ck}}\right) & b \leq -\frac{1}{k} \end{cases} \tag{12}$$

$$FS_{max} = \begin{cases} \dfrac{a(d+3bk+3)\sqrt{\frac{k\left(b(d-2)+b^2(-k)+4c^2k\right)+d-1}{ck}}}{8\sqrt{2}\sqrt{c}\sqrt{k}} & b \geq -\frac{1}{k} \\ \dfrac{a(d-3bk-3)\sqrt{-\frac{k\left(b(d+2)+b^2k-4c^2k\right)+d+1}{ck}}}{8\sqrt{2}\sqrt{c}\sqrt{k}} & b \leq -\frac{1}{k} \end{cases} \tag{13}$$

where, it has to be noted that the analytical expression of Equations 12–13 have to be evaluated for both (i) and $(i+1)$ load cycles and, then, the FS CP factor is selected as the solution having the maximum (always positive) value.
As it can be observed, both ω_{max} and FS_{max} are characterised by a C^0-type continuity condition at $b = -\frac{1}{k}$. An example of the solution for a structural steel having $S_y = 355\,\text{MPa}$ is given in Figure 3. The solution is given for two fixed values of the material constant $k = 0.1$ and $k = 1$, which represent typical extreme values for that parameter. The stress-strain state involved in the loading cycle is described by parameters a, b, c given in previous eq. 10; in other words, each point on the surface represent a different fatigue load cycle.

Figure 3a and Figure 3b report the ω_{max} function, while the FS_{max} function is shown in Figure 3c and Figure 3d for $k = 0.1$ and $k = 1$, respectively. It can be observed how the ω_{max} solution can be represented through an individual surface, being independent of the value of a, i.e. on the shear strain range.
On the other hand, the FS parameter is strongly influenced by the shear strain range, represented by parameter a and moderately influenced by parameter b representing the normalised radius of the largest stress circle. The influence of parameter c on the FS parameter is much lower in all the domain. The effect of k can be clearly noticed, for $b = -\frac{1}{k}$, in all the plots.
Once the critical plane factor FS_{max} has been obtained, the critical plane orientation can also be derived. The rotation matrix to be considered is given in Equation 14 and it is obtained by multiplying the rotation matrix R_p (i.e., representing the matrix containing the direct cosines of the principal directions), with the rotation matrix R_y (i.e., representing the rotation matrix around y-axis of an angle ω_{max}).

$$R = R_p R_y(\omega_{max}) = \begin{bmatrix} | & | & | \\ \mathbf{n_1}^{(i),(i+1)} & \mathbf{n_2}^{(i),(i+1)} & \mathbf{n_3}^{(i),(i+1)} \\ | & | & | \end{bmatrix} \begin{bmatrix} \cos(\omega_{max}) & 0 & \sin(\omega_{max}) \\ 0 & 1 & 0 \\ -\sin(\omega_{max}) & 0 & \cos(\omega_{max}) \end{bmatrix} \tag{14}$$

In order to enable a direct graphical comparison between the analytical formulation and the plane scanning method, the same rotation sequence of Equation 3 can be employed, as presented in the following:

$$R = R_z(\psi)R_y(\theta) = \begin{bmatrix} r_{11} & r_{12} & r_{13} \\ r_{21} & r_{22} & r_{23} \\ r_{31} & r_{32} & r_{33} \end{bmatrix} \tag{15}$$

On the basis of Equation 3, 14 and Equation 15, it is now trivial to obtain the two angles (θ and ψ) in analytical form as shown in Equation 16.

$$\begin{aligned} \theta &= \text{arctan2}(\sqrt{r_{13}^2 + r_{23}^2}, r_{33}) \\ \psi &= \text{arctan2}(r_{23}, r_{13}) \end{aligned} \tag{16}$$

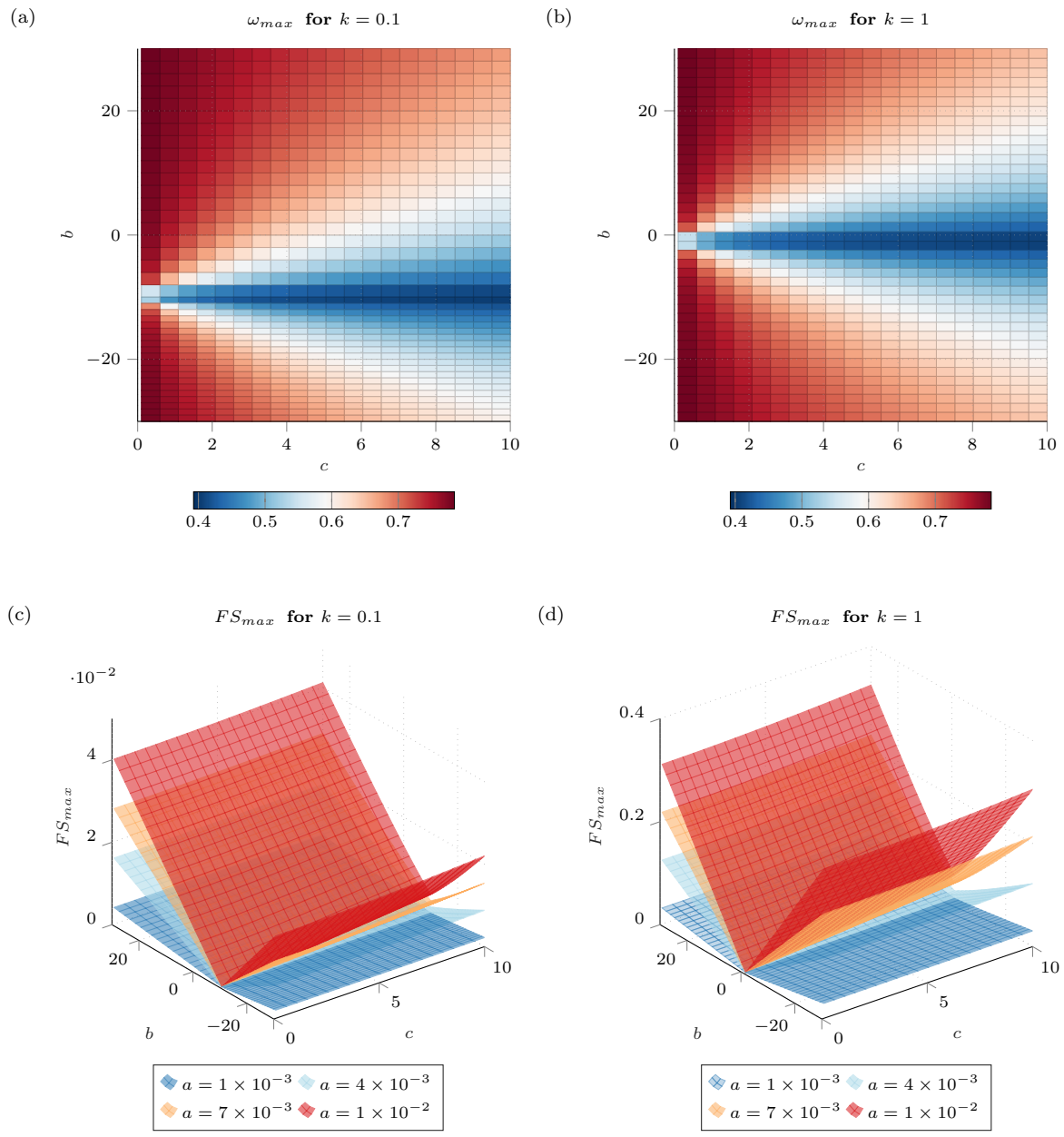

Figure 3: Surface plots of ω_{max} and FS_{max} functions; a) ω_{max} for $k = 0.1$, b) ω_{max} for $k = 1$, c) FS_{max} for $k = 0.1$ and $a = [0.001, 0.004, 0.007, 0.01]$ and c) FS_{max} for $k = 1$ and $a = [0.001, 0.004, 0.007, 0.01]$

5. Material and method

In order to validate the analytical solution presented in prvious section, three different case studies were selected, to represent a wide range of structural problems that may be found in practical applications. The case studies include an hourglass specimen, a notched specimen, and a welded joint between a pipe and a plate. The hourglass and notched specimens were subjected to tensile-compressive and torsional loading, while the welded joint was subjected to pure bending and pure torsional loading. The technical drawing of the hourglass specimen, based on ASTM E466 with a minimum diameter of 12 mm, is shown in Figure 4a.

5.1. Finite element analysis

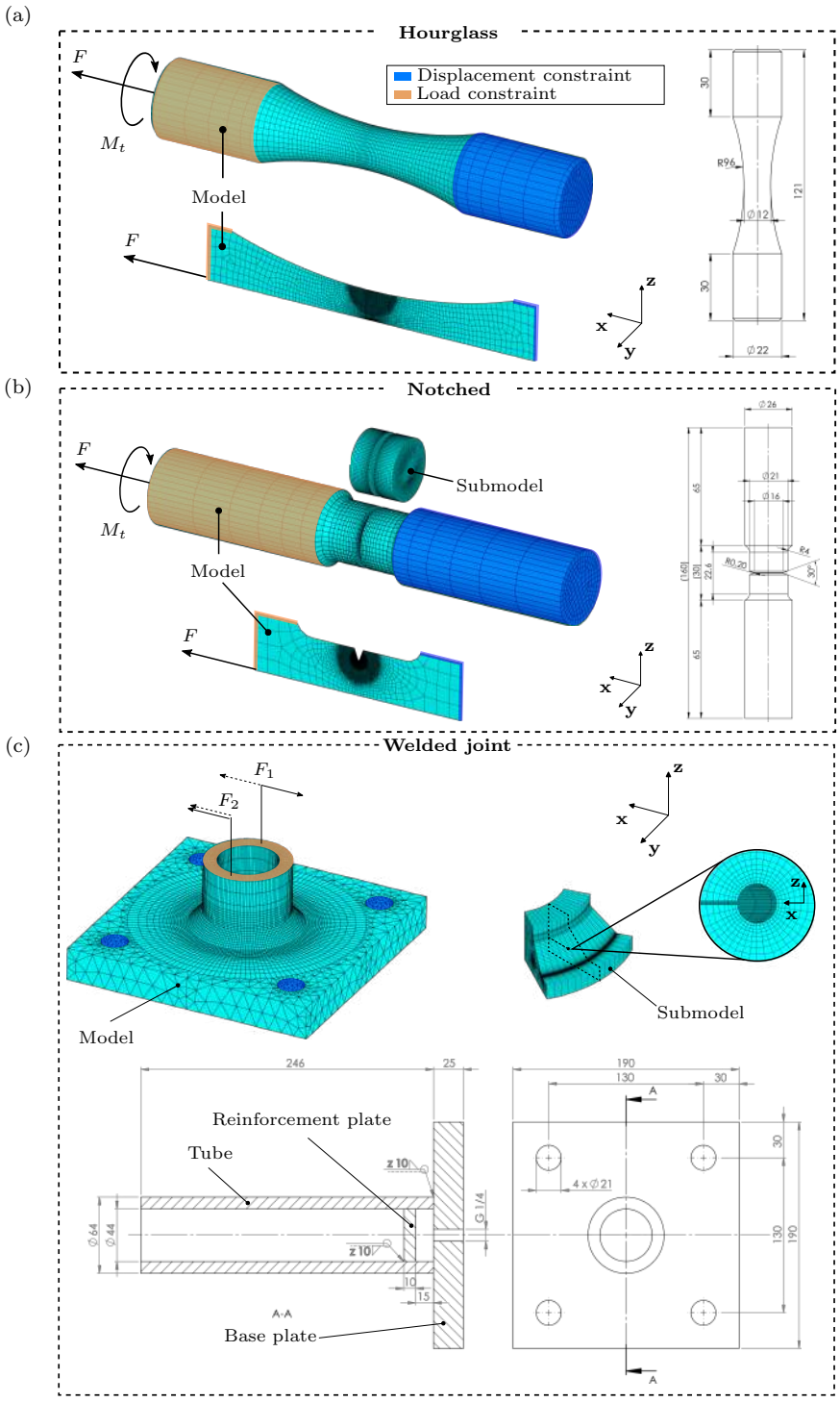

Figure 4: Finite element models and technical drawings of the investigated case studies: (a) hourglass specimen with two-dimensional and three-dimensional model, (b) notched specimen with two-dimensional model, three-dimensional model and submodel, and (c) welded joint with submodel.

The notched specimen geometry, described by a notch radius of 0.2 mm and a minimum diameter of 16 mm, is shown in Figure 4b. Figure 4c shows the welded joint geometry, which consists of a tube, a reinforcement circular plate, and a quadrangular base plate. The seam weld of interest for this work was the one between the tube and the base plate. The welded joint was previously studied by the same authors examining its fatigue endurance under different loading conditions and in the presence of residual stresses [5–7, 41–44]. For all the cases FE-analyses were conducted using the second release of Ansys© 2021 software.Static structural analyses were performed assuming small displacements; structural steel S355 was considered as the material for all three case studies with linear elastic behaviour, $E = 210\,\text{GPa}$ and $\nu = 0.3$. In order to determine the FS critical plane factor, a yield strength $S_y = 355\,\text{MPa}$ and a material constant $k = 0.4$ were considered.

Three-dimensional FE models were used for all loading conditions of the welded joint (Figure 4c) and in the case of torsional loading for both the hourglass specimen (Figure 4a) and the notched specimen (Figure 4b). In this case 3D structural brick elements with 20 nodes and quadratic shape functions were employed. Whereas an axisymmetric assumption was employed together with 2D structural plane elements with 8 nodes and quadratic shape functions in the case of hourglass and notched specimens loaded in tension-compression. The hourglass specimen mesh consisted of 336134 nodes and 81018 elements for the three-dimensional geometry and 24276 nodes and 7991 elements for the two-dimensional geometry, respectively. Submodeling technique was used to optimize the mesh in the notch region, in case of three-dimensional notched specimen model; a number of 123170 nodes and 29234 elements for the three-dimensional model and 351974 nodes and 84900 elements for the submodel were used, respectively. The two-dimensional notched specimen model consists of 38897 nodes and 12888 elements. The welded joint, consisting of 96420 nodes and 97728 elements, likewise utilizes the submodel analysis to better describe the stress and strain state in the weld bead region. The submodel included a model slice of 54° opening angle and 155454 nodes and 35408 elements. The mesh size for all FE models was achieved after a convergence analysis. The convergence was reached once a difference lower than 3% was attained on the maximum von Mises stress.

The proportional loading were obtained by applying forces or moments together with fixed supports on the appropriate model surfaces. In the case of hourglass and notched specimens, the cylindrical surfaces of Figure 4d–e were used for applying the boundary conditions, while the top tube surface and the plate holes were used in the case of the welded joint.

The load sequences reported in Tables 1–2 were applied, consisting of two proportional loading conditions. Each column of the table reports the combination of forces/moment applied to a specific specimen geometry in a particular load step of the FE-simulation.

Load type	*Hourglass specimen*		*Notched specimen*		*Welded joint*	
	Load step n.1	Load step n.2	Load step n.1	Load step n.2	Load step n.1	Load step n.2
Case 1	F =18 kN M_t =0 N m	F =74 kN M_t =0 N m	F =1.6 kN M_t =0 N m	F =16 kN M_t =0 N m	F_1 =−5.7 kN F_2 =−5.7 kN	F_1 =5.7 kN F_2 =5.7 kN
Case 2	F =0 kN M_t =7.5 N m	F =0 kN M_t =75 N m	F =0 kN M_t =8 N m	F =0 kN M_t =63 N m	F_1 =−15 kN F_2 =15 kN	F_1 =15 kN F_2 =−15 kN

Table 1: Load steps combination used during simulations with F referring to the applied force and M_t referring to the torque shown in Figure 4

Load type	*Hourglass specimen*	*Notched specimen*	*Welded joint*
Case 1	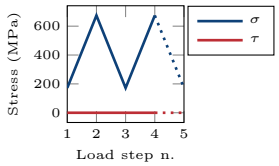	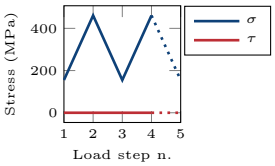	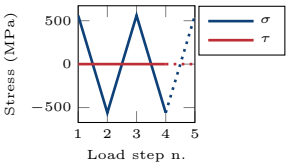
Case 2	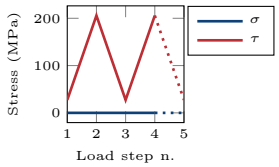	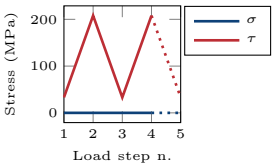	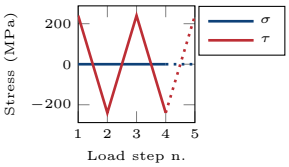

Table 2: Graphical overview of the main normal and shear stress components pattern over load steps

6. Results

In this section the results obtained by closed form solution of the FS CP factor are discussed in comparison with those obtained by the standard plane scanning method. The functions presented in section 4 provide the essential mathematical background to apply the analytical method; the CP factor solutions resulting from the above functions furnish the results explicitly, yielding a precise solution rather than a numerical approximation.

Figure 5 provides a graphical comparison of CP orientation and CP values between the two methods for the three different loading cases presented in previous section, including the hourglass specimen, notched specimen, and welded joint. The tensile loading case for the hourglass and notched specimens, as well as the bending loading for the welded joint, are shown in Figures 5a-5c, while the torsional loading cases are presented in Figures 5d-5f, respectively. The CP orientation identified by the new method is represented by a white dot in all the Figures. As it can be observed the closed form solution perfectly fits with the maximum values of the colored plots, which represent the $FS(\theta, \psi)$ values derived from the spatial plane scanning method. Although the surfaces often exhibit periodic patterns within the angular range, the solution found by the proposed closed form solution is unique, and the periodicity information can be obtained by considering the loading case and the symmetry of the stress tensor, as described by Cauchy's stress tensor. The values of parameters a, b and c are reported in Table 3 for the case-studies presented in Figure 5a–f.

Case study	a	b	c
Hourglass – Tensile	0.0017	0.9729	0.9731
Notched – Tensile	0.0121	0.7041	0.6218
Welded joint – Bending	0.0046	0.8835	0.8296
Hourglass – Torsion	0.0018	0	0.0843
Notched – Torsion	0.0015	0	0.7415
Welded joint – Torsion	0.0043	0	0.7903

Table 3: Parameter values required to calculate the FS closed-form solution for all case studies described in Figure 5

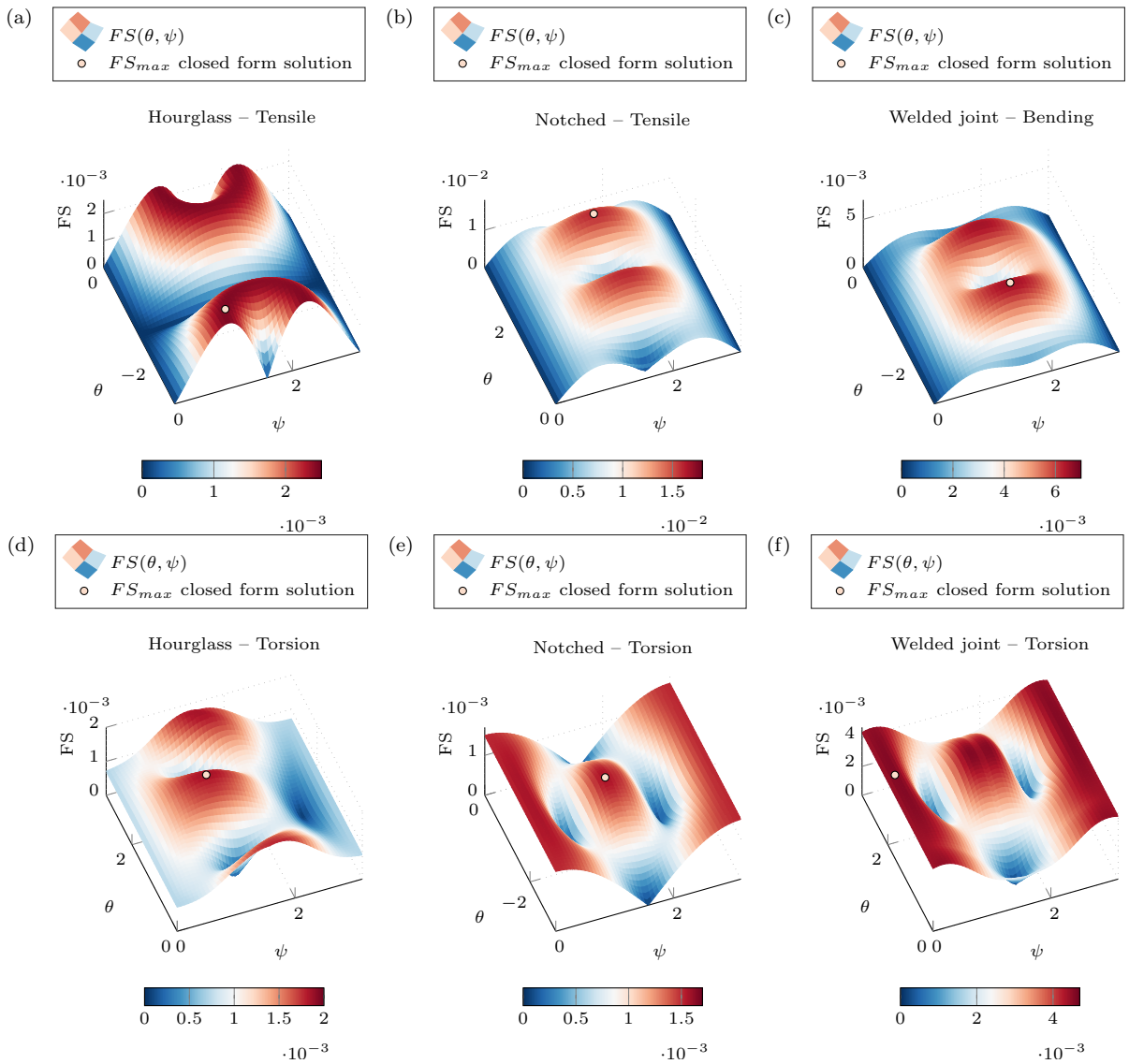

Figure 5: Comparison of FS solutions derived from the standard plane scanning method ($FS(\theta,\psi)$) and that derived from the closed-form procedure (FS_{max}) for (a) the hourglass specimen subjected to tensile loading, (b) the notched specimen subjected to tensile loading, (c) the welded joint subjected to bending loading, (d) the hourglass specimen subjected to torsion loading, (e) the notched specimen subjected to torsion loading and (f) the welded joint subjected to torsion loading.

The improvement in computing time is illustrated in Table 4. All codes were executed in the Matlab® environment on an 11th Gen Intel(R) Core(TM) i7 with 16GB of available RAM and 4 cores. The performance index PI defined in Equation 17 was used to compare the computational efficiency of the closed form solution, to the standard plane scanning method. In Equation 17, t_{cs} represents the computation time required by the closed form solution, while t_{ps} represents the computation time required by the plane scanning procedure. PI is 100% when the computation time with the analytical solution is zero, or when the computation time required by the plane scanning method is infinite, and 0% when there is no reduction in computing time, i.e. $t_{cs} = t_{ps}$. The significant time reduction is caused by avoiding multiple plane scanning in space while providing the exact solution. As it can be observed, significant time reduction was achieved,

with the PI parameter consistently exceeding 99.8%.

$$PI = \left(1 - \frac{t_{cs}}{t_{ps}}\right) \tag{17}$$

The computational time was significantly decreased from approximately 2 s to around 2×10^{-3} s by implementing a non-optimized code in Matlab®. With further optimization through the use of lower-level programming languages, additional reductions in computational time are likely to be achievable. This huge increment in coputation efficiency suggests the possibility the CP method also for complex geometries, when the critical locations are not known in advance.

Computational time comparison									
Load type	*Hourglass specimen*			*Notched specimen*			*Welded joint*		
	t_{cs}	t_{ps}	PI	t_{cs}	t_{ps}	PI	t_{cs}	t_{ps}	PI
Case 1	2.15×10^{-3} s	2.21 s	99.9%	2.84×10^{-3} s	2.006 s	99.8%	2.47×10^{-3} s	1.849 s	99.8%
Case 2	1.822×10^{-3} s	2.27 s	99.9%	1.985×10^{-3} s	2.282 s	99.9%	2.04×10^{-3} s	2.164 s	99.9%

Table 4: Comparison of computational cost between the closed form solution and the standard plane scanning method

It is worth noting that if any of the assumptions given in section 4 is not holding, a closed form solution cannot be obtained. Figure 6 provides a practical example in which a non-proportional loading condition was applied to the hourglass specimen. Specifically, a first load step with $F = 76$ kN and $M_t = 0$ N m and a second load step with $F = 0$ kN and $M_t = 100$ N m. Under these conditions a significant difference in FS_{max} results can be found both in terms of FS parameter and in terms of the critical plane orientation, as given by θ and ψ. Figure 6a represents the closed form solution compared with maximum value derived from the standard spatial plane scanning method. For this specific case, an error of 13.4% on the modulus of FS and a maximum error of 0.24 rad on the angular position of the plane is obtained. It may also result interesting to notice how the maximum error in FS value is achieved in the critical region of the component, as shown in Figure 6b. As it can be reasonably expected, this confirms how the application of the closed form solution is not conservative when either one of the underlying hypotheses are not met.

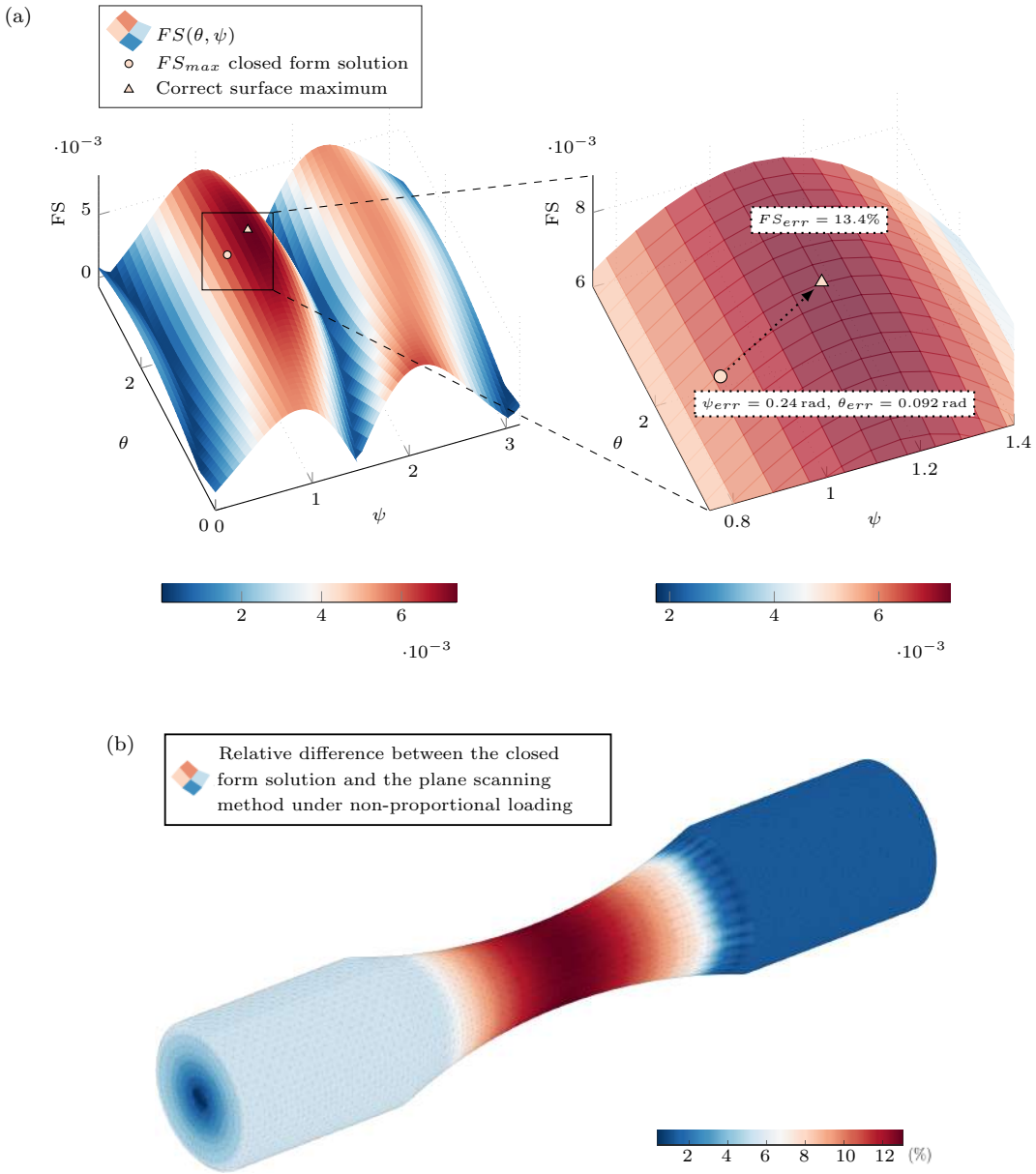

Figure 6: Non-proportional loading case on the hourglass specimen; (a) comparison of FS solutions derived from the plane scanning method ($FS(\theta, \psi)$) and the closed form solution (FS_{max}), (b) relative error map between the closed form solution and the correct maximum solution of $FS(\theta, \psi)$ per each node.

7. Conclusions

Following a previous work by the authors, the purpose of the present study was to develop a closed form solution for the FS CP factor in its more general formulation, including the shear strain range and the maximum stress acting on the plane during the loading cycle. The method utilizes stress and strain tensor invariants and coordinates transformation law and was implemented in a readily available Matlab® script. The closed form solution was discussed with reference to its graphical representation for a structural steel and similar solutions can be easily obtained for different metallic materials. Various case studies were analysed and discussed in comparison to the standard plane scanning method, to provide a wide range

of component geometries and loading conditions. From the performed analyses and results obtained, the following conclusions can be drawn:

- the method can be used for uniaxial and multiaxial proportional loading conditions, under linear-elastic material behaviour;
- the method offers a huge speed up in solution time, with respect to the standard plane scanning method, with a reduction of computation time greater than 99.8% on a single node, for the examined test cases, where a 1° resolution in plane orientation was selected; this reduction in computation time could potentially make CP methods easier and more attactive to be used, even in and industrial context;
- the proposed method provides a closed-form solution for the critical plane and, consequently, for the damage parameter, compared to the standard plane scanning method;
- the method is easy to use and can be implemented in a variety of codes since it utilizes basic tensor math; the extension to other CP factors likely appears to be straightforward.

Reducing computation time during the post-processing phase is crucial for evaluating damage factors, as it enables a more detailed and complete evaluation of the studied model, even in case of complex geometries with FE models made with large number of nodes.

Acknowledgement

Financed by the European Union - NextGenerationEU (National Sustainable Mobility Center CN00000023, Italian Ministry of University and Research Decree n. 1033 - 17/06/2022, Spoke 11 - Innovative Materials & Lightweighting). The opinions expressed are those of the authors only and should not be considered as representative of the European Union or the European Commission's official position. Neither the European Union nor the European Commission can be held responsible for them.

References

[1] Bhaumik SK, Sujata M, Venkataswamy MA. Fatigue failure of aircraft components. *Eng Fail Anal.* 2008;15:675–694.
[2] Kuncham E, Sen S, Kumar P, Pathak H. An online model-based fatigue life prediction approach using extended Kalman filter. *Theor Appl Fract Mech.* 2022;117:103143.
[3] Palmieri M, Zucca G, Morettini G, Landi L, Cianetti F. Vibration Fatigue of FDM 3D Printed Structures: The Use of Frequency Domain Approach. *Materials.* 2022;15:854.
[4] Chen F, Shang DG, Li DH, Wang LW. Multiaxial thermo-mechanical fatigue life prediction based on notch local stress-strain estimation considering temperature change. *Eng Fract Mech.* 2022;265:108384.
[5] Frendo F, Marulo G, Chiocca A, Bertini L. Fatigue life assessment of welded joints under sequences of bending and torsion loading blocks of different lengths. *Fract Eng Mater Struct.* 2020;43:1290–1304.
[6] Chiocca A, Frendo F, Bertini L. Evaluation of residual stresses in a tube-to-plate welded joint. *MATEC Web of Conferences.* 2019;300:19005.
[7] Chiocca A, Frendo F, Bertini L. Evaluation of residual stresses in a pipe-to-plate welded joint by means of uncoupled thermal-structural simulation and experimental tests. *Int J Mech Sci.* 2021;199:106401.
[8] Meneghetti G, Campagnolo A, Visentin A, et al. Rapid evaluation of notch stress intensity factors using the peak stress method with 3D tetrahedral finite element models: Comparison of commercial codes. *Fract Eng Mater Struct.* 2022;45:1005–1034.
[9] Lazzarin P, Berto F. Some expressions for the strain energy in a finite volume surrounding the root of blunt V-notches. *Int J Fract.* 2005;135:161–185.
[10] Berto F, Lazzarin P. The volume-based strain energy density approach applied to static and fatigue strength assessments of notched and welded structures. in *Procedia Engineering*;1:155–158No longer published by Elsevier 2009.
[11] Mroziński S. Energy-based method of fatigue damage cumulation. *Int J Fatigue.* 2019;121:73–83.
[12] Varvani-Farahani A, Haftchenari H, Panbechi M. An energy-based fatigue damage parameter for off-axis unidirectional FRP composites. *Compos Struct.* 2007;79:381–389.
[13] European Committee for Standardization . Eurocode 3: Design of steel structures — Part 1-9: Fatigue. *(CEN).* 2005;50:77.
[14] Hobbacher AF. The new IIW recommendations for fatigue assessment of welded joints and components - A comprehensive code recently updated. *Int J Fatigue.* 2009;31:50–58.

[15] Karakaş , Zhang G, Sonsino CM. Critical distance approach for the fatigue strength assessment of magnesium welded joints in contrast to Neuber's effective stress method. *Int J Fatigue.* 2018;112:21–35.
[16] Taylor D, Barrett N, Lucano G. Some new methods for predicting fatigue in welded joints. *Int J Fatigue.* 2002;24:509–518.
[17] Radaj D, Sonsino CM, Fricke W. *Fatigue Assessment of Welded Joints by Local Approaches: Second Edition* . 2006.
[18] Fatemi A, Socie DF. A critical plane approach to multiaxial fatigue damage including out-of-phase loading. *Fract Eng Mater Struct.* 1988;11:149–165.
[19] Findley WN. A Theory for the Effect of Mean Stress on Fatigue of Metals Under Combined Torsion and Axial Load or Bending. *J eng ind.* 1959;81:301–305.
[20] Kandil FA, Brown MW, J. MK. Biaxial low-cycle fatigue failure of 316 stainless steel at elevated temperatures. in *Mechanical Behaviour and Nuclear Applications of Stainless Steel at Elevated Temperatures*(London, UK)Maney Pub. 1982.
[21] Socie D. Multiaxial fatigue damage models. *J Eng Mater Technol.* 1987;109:293–298.
[22] Huang J, Yang X, Shi D, Yu H, Dong C, Hu X. Systematic methodology for high temperature LCF life prediction of smooth and notched Ni-based superalloy with and without dwells. *Comput Mater Sci.* 2014;89:65–74.
[23] Reis L, Li B, De Freitas M. A multiaxial fatigue approach to Rolling Contact Fatigue in railways. *Int J Fatigue.* 2014;67:191–202.
[24] Cruces AS, Lopez-Crespo P, Moreno B, Antunes FV. Multiaxial fatigue life prediction on S355 structural and offshore steel using the SKS critical plane model. *Metals.* 2018;8:1060.
[25] El-sayed HM, Lotfy M, El-din Zohny HN, Riad HS. Prediction of fatigue crack initiation life in railheads using finite element analysis. *Ain Shams Eng J.* 2018;9:2329–2342.
[26] Cruces AS, Garcia-Gonzalez A, Moreno B, Itoh T, Lopez-Crespo P. Critical plane based method for multiaxial fatigue analysis of 316 stainless steel. *Theor Appl Fract Mech.* 2022;118:103273.
[27] Marques JME, Benasciutti D, Carpinteri A, Spagnoli A. An algorithm for fast critical plane search in computer-aided engineering durability analysis under multiaxial random loadings: Application to the Carpinteri–Spagnoli–Vantadori spectral method. *Fract Eng Mater Struct.* 2020;43:1978–1993.
[28] Wentingmann M, Noever-Castelos P, Balzani C. An adaptive algorithm to accelerate the critical plane identification for multiaxial fatigue criteria. in *Proceedings of the 6th European Conference on Computational Mechanics: Solids, Structures and Coupled Problems, ECCM 2018 and 7th European Conference on Computational Fluid Dynamics, ECFD 2018*:3745–3754 2020.
[29] Sunde SL, Berto F, Haugen B. Efficient implementation of critical plane for 3D stress histories using triangular elements. *Int J Fatigue.* 2020;134:105448.
[30] Liu J, Ran Y, Wei Y, Zhang Z. A critical plane-based multiaxial fatigue life prediction method considering the material sensitivity and the shear stress. *Int J Press Vessels Pip.* 2021;194:104532.
[31] Albinmousa J, Al Hussain M. Polar damage sum concept for constant amplitude proportional and nonproportional multiaxial fatigue analysis. *Forces in Mechanics.* 2021;4:100025.
[32] Ma TH, Zhou CY, Gao N, Chang L, He XH. Low cycle fatigue behavior of CP-Ti under multiaxial load-controlled mode at different multiaxial stress ratios. *Int J Fatigue.* 2022;160:106868.
[33] Chiocca A, Frendo F, Marulo G. An efficient algorithm for critical plane factors evaluation. *Int J Mech Sci.* 2023;242:107974.
[34] Jiang Y, Hertel O, Vormwald M. An experimental evaluation of three critical plane multiaxial fatigue criteria. *Int J Fatigue.* 2007;29:1490–1502.
[35] Olausson K. *Material Data Derivation For The Fatemi And Socie Critical Plane Method.* PhD thesis 2007.
[36] Lopez-Crespo P, Moreno B, Lopez-Moreno A, Zapatero J. Study of crack orientation and fatigue life prediction in biaxial fatigue with critical plane models. *Eng Fract Mech.* 2015;136:115–130.
[37] Yu ZY, Zhu SP, Liu Q, Liu Y. Multiaxial fatigue damage parameter and life prediction without any additional material constants. *Materials.* 2017;10:923.
[38] Zhu SP, Yu ZY, Correia J, De Jesus A, Berto F. Evaluation and comparison of critical plane criteria for multiaxial fatigue analysis of ductile and brittle materials. *Int J Fatigue.* 2018;112:279–288.
[39] Yang S, Sun J. Multiaxial fatigue life assessment of 304 austenitic stainless steel with a novel energy-based criterion. *Int J Fatigue.* 2022;159:106728.
[40] Fatemi A, Kurath P. Multiaxial fatigue life predictions under the influence of mean-stresses. *J Eng Mater Technol.* 1988;110:380–388.
[41] Chiocca A, Frendo F, Bertini L. Evaluation of heat sources for the simulation of the temperature distribution in gas metal arc welded joints. *Metals.* 2019;9:1142.
[42] Chiocca A, Frendo F, Bertini L. Experimental evaluation of relaxed strains in a pipe-to-plate welded joint by means of incremental cutting process. *Procedia Struct.* 2020;28:2157–2167.
[43] Chiocca A, Frendo F, Aiello F, Bertini L. Influence of residual stresses on the fatigue life of welded joints. Numerical simulation and experimental tests. *Int J Fatigue.* 2022;162:106901.
[44] Chiocca A. *Influence of residual stresses on the fatigue life of welded joints.* PhD thesisUniversity of Pisa 2021.